Neurobiology of Aging 34 (2013) 1759–1771

Contents lists available at SciVerse ScienceDirect

Neurobiology of Aging

journal homepage: www.elsevier.com/locate/neuaging

# Unfolded protein response activates glycogen synthase kinase-3 via selective lysosomal degradation

Diana A.T. Nijholt [a,1], Anna Nölle [a,1], Elise S. van Haastert [b], Hessel Edelijn [a], Ruud F. Toonen [c], Jeroen J.M. Hoozemans [b], Wiep Scheper [a,d,*]

[a] Department of Genome Analysis, Academic Medical Center, University of Amsterdam, Amsterdam, the Netherlands
[b] Department of Pathology, Neuroscience Campus Amsterdam, VU University Medical Center, Amsterdam, the Netherlands
[c] Department of Functional Genomics, Center for Neurogenomics and Cognitive Research, Neuroscience Campus Amsterdam, Vrije Universiteit Amsterdam (VUA), Amsterdam, the Netherlands
[d] Department of Neurology, Academic Medical Center, University of Amsterdam, Amsterdam, the Netherlands

ARTICLE INFO

*Article history:*
Received 13 March 2012
Received in revised form 20 December 2012
Accepted 12 January 2013
Available online 14 February 2013

*Keywords:*
Alzheimer's disease
Unfolded protein response
Tau pathology
Phosphorylation
Glycogen synthase kinase 3
Lysosome
Autophagy

ABSTRACT

The unfolded protein response (UPR) is a stress response that is activated upon disturbed homeostasis in the endoplasmic reticulum. In Alzheimer's disease, as well as in other tauopathies, the UPR is activated in neurons that contain early tau pathology. A recent genome-wide association study identified genetic variation in a UPR transducer as a risk factor for tauopathy, supporting a functional connection between UPR activation and tau pathology. Here we show that UPR activation increases the activity of the major tau kinase glycogen synthase kinase (GSK)-3 in vitro via a selective removal of inactive GSK-3 phosphorylated at $Ser^{21/9}$. We demonstrate that this is mediated by the autophagy/lysosomal pathway. In brain tissue from patients with different tauopathies, lysosomal accumulations of $pSer^{21/9}$ GSK-3 are found in neurons with markers for UPR activation. Our data indicate that UPR activation increases the activity of GSK-3 by a novel mechanism, the lysosomal degradation of the inactive $pSer^{21/9}$ GSK-3. This may provide a functional explanation for the close association between UPR activation and early tau pathology in neurodegenerative diseases.



## 1. Introduction

Aggregates of the microtubule associated protein tau are found in several neurodegenerative disorders, commonly referred to as tauopathies. This includes Alzheimer's disease (AD), Pick's disease (PiD), progressive supranuclear palsy (PSP), and frontotemporal dementia and parkinsonism linked to chromosome 17 (FTDP-17) (Ballatore et al., 2007; Gendron and Petrucelli, 2009), a familial tauopathy that is associated with mutations in the gene encoding tau. Tau is predominantly involved in facilitating the structure and function of microtubules. Under physiological conditions, tau phosphorylation is a rapid and reversible process, mediated by the opposing actions of several protein kinases and phosphatases (Cowan et al., 2010; Cuchillo-Ibanez et al., 2008). In contrast, hyperphosphorylation of tau is thought to precede the formation of tau aggregates and is therefore associated with pathology (Alonso et al., 2001; Alonso et al., 2010; Bancher et al., 1989; Rankin et al., 2008).

The unfolded protein response (UPR), a stress response pathway that is activated upon a disturbance in endoplasmic reticulum (ER) homeostasis, is strongly associated with the pathology of tauopathies (Hoozemans et al., 2009; Nijholt et al., 2011c). Three ER transmembrane proteins function as stress sensors and mediate the effects of the UPR: PERK, IRE1, and ATF6. During ER stress, these proteins are activated by phosphorylation (PERK and IRE1) or cleavage (ATF6), and activate responses aimed at restoring homeostasis in the ER (Schroder and Kaufman, 2005). Activation of the UPR leads to the following: an overall reduction in translation to reduce the amount of novel polypeptides in the ER, and the transcriptional and translational upregulation of factors that facilitate protein folding and degradation. We and others previously reported UPR activation markers in close spatio-temporal connection with phosphorylated tau in AD brain (Hoozemans et al., 2005; Hoozemans et al., 2009; Unterberger et al., 2006). Our group observed the same association of the UPR and phosphorylated tau protein in non-AD tauopathies, including cases of sporadic PiD, PSP, and FTDP-17 (Nijholt et al., 2011c). In this cohort, the involvement of amyloid β (Aβ) pathology and overall ageing effects could be excluded,

* Corresponding author at: Department of Genome Analysis, Academic Medical Center, P.O.Box 22660, 1100 DE Amsterdam, The Netherlands. Tel.: +31-20-5664959; fax: +31-20-5669312.
*E-mail address:* w.scheper@amc.uva.nl (W. Scheper).
[1] D.A.T.N. and A.N. contributed equally to this work.

0197-4580 
http://dx.doi.org/10.1016/j.neurobiolaging.2013.01.008

strengthening the connection between the UPR and early tau pathology. Interestingly, a recent genome-wide association study has identified genetic variation in the gene encoding the ER stress transducer PERK as a risk factor for PSP, suggesting that perturbation of the UPR can influence the risk for developing tau pathology (Hoglinger et al., 2011).

A large number of kinases phosphorylate tau in vitro (Hanger et al., 2009), but the precise mechanisms of physiological regulation have not yet been elucidated. A major kinase implicated in physiological and pathological phosphorylation of tau is glycogen synthase kinase 3 (GSK-3). Tau is phosphorylated by GSK-3 in vitro (Hanger et al., 1992; Ishiguro et al., 1992), in cultured cells (Lovestone et al., 1994; Lovestone et al., 1996), and in transgenic mice overexpressing GSK-3 (Brownlees et al., 1997; Gomez-Sintes et al., 2007; Lucas et al., 2001). GSK-3 phosphorylates tau at multiple sites, and most of these sites are also phosphorylated in disease (Hanger et al., 1992; Hanger and Noble, 2011; Wagner et al., 1996). GSK-3 plays a role in a wide variety of signaling pathways including glycogen metabolism, protein synthesis, mitosis, apoptosis, and microtubule dynamics (Forde and Dale, 2007). GSK-3 exists as 2 highly homologous isoforms, GSK-3α and GSK-3β, which are encoded by different genes located on chromosomes 19 and 3, respectively (Woodgett, 1990). Both isoforms are expressed in the brain (Lau et al., 1999; Yao et al., 2002), however GSK-3β appears to be the predominantly expressed isoform (Lau et al., 1999). Some, but not all, substrates require priming by phosphorylation at a nearby residue by another kinase that enables phosphorylation by GSK-3 (Bax et al., 2001; Fiol et al., 1987). GSK-3β phosphorylates tau at primed and unprimed sites; however, phosphorylation at primed sites was shown to play a key role in regulating in vitro tau microtubule binding (Cho and Johnson, 2003). GSK-3 activity is inhibited by phosphorylation of the $Ser^{21}$ and $Ser^{9}$ residue in GSK-3α/β, respectively. This residue is located in the N-terminus of GSK-3; when phosphorylated, this acts as a primed pseudo-substrate that loops back in the active site (Forde and Dale, 2007). Inhibitory phosphorylation of GSK-3 at this site occurs in response to several signaling pathways. Protein kinase A phosphorylates GSK-3 upon an increase in levels of the second messenger cyclic AMP, caused by binding of ligands to G-protein–coupled receptors on the cell membrane (Fang et al., 2000). The insulin signaling pathway leads to increased activity of phosphatidyl inositol kinase 3 (PI3K) and protein kinase B (PKB)/Akt. The commonly used activator of GSK-3, wortmannin (Wm), inhibits PI3K and in this manner prevents inhibitory phosphorylation by PKB/Akt (Grimes and Jope, 2001; Li et al., 2006). Phosphorylation of GSK-3α/β at $Tyr^{216}$ and $Tyr^{279}$, respectively, is associated with increased GSK-3 activity (Bax et al., 2001). Inhibition of this phosphorylation event either by enzymatic dephosphorylation or mutation of Tyr into Phe, decreases the kinase activity (Hagen et al., 2002). Phosphorylation at the Tyr residue is suggested to be an autophosphorylation event; however, some kinases have been shown to target GSK-3 $Tyr^{216/279}$ in vitro (Hartigan et al., 2001; Lesort et al., 1999; Medina and Wandosell, 2011). The precise mechanism remains unknown but the position of the $Tyr^{216/279}$ residue in the GSK-3 activation loop suggests it induces a conformational change that results in more efficient substrate binding (Bax et al., 2001; Hagen et al., 2002).

The role of GSK-3 in tau pathology has been the subject of several studies; however, its regulation and involvement in the pathogenesis of tauopathies is not yet fully elucidated. GSK-3β co-isolates with brain-derived microtubules (Ishiguro et al., 1993) and, in cells, phosphorylates tau at epitopes also found in AD (Hanger et al., 1992; Lovestone et al., 1994). Inhibition by lithium or more specific GSK-3 inhibitors have prevented tau phosphorylation and aggregation in several murine models (Leroy et al., 2010; Noble et al., 2005; Sereno et al., 2009). The association of the UPR with early tau pathology prompted the investigation of effects of in vitro UPR induction on GSK-3 activity. Chemical induction of the UPR results in decreased phosphorylation at the inhibitory $Ser^{21/9}$ epitope and increased phosphorylation at the activating $Tyr^{279/216}$ epitope (Fu et al., 2010). Another study identified only decreased $Ser^{21/9}$ phosphorylation (Song et al., 2002). Although the mechanism remains elusive, these studies suggest that activation of the UPR leads to increased activity of GSK-3.

In this study, we further investigated the connection between activation of the UPR and GSK-3 activity in vitro. Furthermore, we analyzed the presence of GSK-3 in connection to UPR activation and tau pathology in post-mortem brain material from patients with different types of tauopathies. Our data provide evidence for UPR-induced regulation of GSK-3 activity via lysosomal degradation.

## 2. Methods

### 2.1. Cell culture, differentiation, and treatment

Human SK-N-SH neuroblastoma cells were cultured in Dulbecco's modified Eagle's medium with GlutaMax (Gibco BRL, Carlsbad, CA) supplemented with 10% fetal calf serum (Lonza, Basel, Switzerland) and 100 U/mL penicillin (Yamanouchi Pharma BV, Leiderdorp, the Netherlands). Cells were differentiated in culture medium supplemented with all trans-retinoic acid (Sigma, St Louis, MO) in a final concentration of 10 μmol/L for 5 days. Differentiated cells were subsequently treated with tunicamycin (Tm), lithium chloride (LiCl), and Bafilomycin (BAF) at indicated concentrations for 16 hours. Treatment with wortmannin (Wm) was performed at 100 nmol/L for 1 hour before harvest. For starvation, medium was removed and cells were washed twice in phosphate-buffered saline (PBS) to remove excess nutrients. Cells were subsequently cultured for 2 hours in Earle's balanced salt solution (Sigma), which lacks essential amino acids.

Dissociated cortical neurons were prepared from embryonic day 18 mice as described elsewhere (De Wit et al., 2009). Cerebral cortices were dissected in Hanks Buffered Salts Solution (HBSS, Sigma) and digested with 0.25% trypsin (Invitrogen Life Technologies, Carlsbad, CA, USA) for 20 minutes at 37 °C. Tissue was washed and triturated with fire-polished Pasteur pipettes, counted, and plated in 6-well plates (200,000 neurons per well) in Neurobasal medium supplemented with 2% B-27, 1.8% HEPES, 1% glutamax, and 1% Pen-Strep (all from Invitrogen). For immunocytochemistry, high-density cultures (25,000 neurons per well) were plated on pre-grown cultures of rat glia cells (37,500 cells per well) on 18-mm glass coverslips in 12-well plates. Neurons were treated with Tm at DIV7.

### 2.2. ELISA colorimetric assay

The InCell ELISA colorimetric assay (Thermo Scientific, Waltham, MA) was performed according to the manufacturer's recommendations. In short, SK-N-SH cells were plated in 96-well plates (15,000 cells per well) and differentiated as described above. All conditions were assayed in triplicate. Unless otherwise stated, all incubations were performed at room temperature (RT) with gentle rocking. Cells were fixed in 4% formaldehyde for 15 minutes. Formaldehyde was aspirated; cells were washed twice in 1x Tris buffered saline (TBS) and incubated with permeabilization buffer for 15 min. After permeabilization, cells were washed with 1x TBS and incubated with quenching solution (containing $H_2O_2$) for 20 minutes. Cells were washed with 1x TBS and subsequently blocked for 30 minutes in blocking solution. After blocking, cells were incubated with the primary antibody solution for 16 hours at 4 °C. Antibodies and their dilutions are described in Table 1. Cells were washed 3 times with wash buffer and subsequently incubated with

**Table 1**
Primary antibodies used in this study

| Antibody | Species | Dilutions | | | | Source |
|---|---|---|---|---|---|---|
| | | IHC single/double | InCell ELISA | Western blot | IF | |
| pPERK | Rabbit | –/1:800 | – | – | – | Santa Cruz Biotechnology, Santa Cruz, CA |
| AT8 | Mouse | 1:1000/1:100 | – | – | – | Pierce, Rockford, IL |
| GSK-3 | Rabbit | 1:500/1:50 | 1:200 | 1:1000 | 1:100 | Cell Signalling Technology, Danvers, MA |
| $pSer^{21/9}$ GSK-3 | Rabbit | 1:100/1:10 | 1:100 | – | – | Cell Signalling Technology |
| $pTyr^{216/279}$ GSK-3 | Mouse | 1:100 | – | – | – | Millipore, Billerica, MA |
| BiP | Goat | – | 1:100 | – | – | Santa Cruz Biotechnology |
| Cathepsin D | Mouse | –/1:1000 | – | – | – | Millipore |
| LAMP1 | Mouse | – | – | – | 1:100 | Santa Cruz Biotechnology |
| LAMP1 | Rat | – | – | – | 1:200 | Biolegend, San Diego, CA |
| eEF2α | Rabbit | – | – | 1:1000 | – | Cell Signalling |
| GAPDH | Mouse | – | – | 1:1000 | – | Millipore |

Key: ELISA, enzyme-linked immunosorbent assay; IF, immunofluorescence; IHC, immunohistochemistry.

diluted HRP conjugate (α-mouse/rabbit for GSK-3 antibodies, α-goat for BiP antibody) for 30 minutes. Cells were washed, and signal was developed by addition of 3,3′,5,5′-tetramethylbenzidine (TMB) substrate. The reaction was stopped when blue color was visible. Absorbance (A) was measured at 450 nm using a FLUOstar Omega microplate reader (BMG Labtech GmbH, Ortenberg, Germany). To correct for variation in the amount of cells, Janus Green whole cell stain was used. Cells were incubated with Janus Green whole cell stain for 5 minutes and subsequently washed with ultrapure water until all excess stain was removed. Elution buffer was added and cells were incubated for 10 minutes before absorption was measured at 615 nm. The A 450-nm values were normalized to A 615-nm values. The normalized A 450-nm values were used to calculate fold changes in assayed protein levels.

### 2.3. Western bloting

SK-N-SH cells were harvested by scraping in 1% (*v/v*) Triton/PBS lysis buffer and neurons by scraping in RIPA lysis buffer (50 mmol/L Tris pH 7.6, 150 mmol/L NaCl, 1% NP-40, 0,5% sodium deoxycholate, 0,1% SDS, 2 mmol/L EDTA) supplemented with Complete protease inhibitors and PhosSTOP (Roche Diagnostics, Mannheim, Germany). Cell lysates were incubated for at least 15 minutes at 4 °C and centrifuged at 20.000× *g* for 20 minutes at 4 °C. Supernatant protein concentration was determined by Bio-Rad Protein Assay (Bio-Rad, Hercules, CA) or BCA (Thermo Scientific, Rockford, IL). Equal amounts of protein were loaded in each lane on a 10% SDS gel. Proteins were blotted onto nitrocellulose membrane using a semi-dry blotting apparatus. Membrane was washed with TBST (0.05% Tween-20 in TBS), blocked with 5% Bovine serum albumin (BSA) in TBS-T (blocking solution) for 1 hour and subsequently incubated with the primary antibody in blocking solution overnight. After washing with TBS-T, membrane was incubated with species-specific secondary antibodies conjugated to horseradish peroxidase (dilution 1:2000, Dako, Glostrup, Denmark) for 1 hour. Membrane was washed and protein signals were visualized using LumiLightPLUS Western blotting substrate (Roche Diagnostics, Mannheim, Germany) and a LAS-3000 luminescent image analyzer (Fuji Photo Film [Europe], Kleve, Germany). Results were analyzed using Advanced Image Data Analyzer software (Raytest, Straubenhardt, Germany) version 3.44.035.

### 2.4. GSK-3 activity assay

GSK-3 activity was measured in crude cell extracts of differentiated SK-N-SH cells using an assay described previously (Ryves et al., 1998). Differentiated SK-N-SH cells were washed once in ice-cold PBS and scraped in ice-cold lysis buffer (50 mmol/L Tris-HCL, pH 8.0, 150 mmol/L NaCl, 5 mmol/L ethylenediaminetetraacetic acid (EDTA), 50 mmol/L NaF, 10 mmol/L DTT, and 1% Triton X-100) supplemented with PhosSTOP phosphatase inhibitor (Roche, Basel, Switzerland) and Protease Inhibitor Cocktail (Roche). Lysates were cleared by centrifugation at 14,000× *g* for 10 minutes. A Bradford protein assay (BioRad, Hercules, CA) was used to determine the protein concentration in each sample.

For each assay, 12.5 μL of cell extract was incubated with 10 μg GSK-3 substrate peptide (Phospho-GS-peptide-2, Upstate Biotechnology, Lake Placid, NY) and 6.25 μL ATP hot mix (200 mmol/L HEPES, pH 7.5, 50 mmol/L $MgCl_2$, 8 mmol/L DTT, 400 μmol/L ATP, and 1 μCi/ μL [$\gamma^{32}$P] ATP (10mCi/mL; Perkin-Elmer, Waltham, MA)). All samples were assayed in the presence and absence of 20 mmol/L LiCl. The substrate peptide used is based on glycogen synthase, a known GSK-3 substrate. The sequence was as follows: *YRAAVPPSPSLSRHSSPHQpSEDEEE*, with p representing the site of the primed phosphate that is necessary for phosphorylation by GSK-3. Assays were incubated at RT and terminated after 8 minutes by spotting onto p81 ion-exchange paper (Whatman GmbH, Dassel, Germany). The membrane was washed 3 times in a large volume of 100 mmol/L phosphoric acid, and bound radioactivity was quantified by scintillation counting. Measured values were corrected for protein content.

### 2.5. Single immunohistochemistry

Post-mortem brain material was obtained from the Netherlands Brain Bank (Table 2). Informed consent was obtained for each patient. Sections (5 μm thick) were mounted onto Superfrost plus tissue slides (Menzel-Gläser, Braunschweig, Germany) and dried overnight at 37 °C. For all stainings, sections were deparaffinized and immersed in 0.3% $H_2O_2$ in methanol for 30 minutes to quench endogenous peroxidise activity. Sections were washed 5 minutes in PBS and treated with 10 mmol/L, pH 6.0, sodium citrate buffer heated by microwave for 10 minutes for antigen retrieval. Sections were subsequently incubated with primary antibody (Table 1) for 16 hours at 4 °C. All primary and secondary antibodies were diluted in PBS containing 1% (w/v) Bovine serum albumin (BSA; Boehringer Ingelheim GmbH, Ingelheim am Rhein, Germany). Negative controls were created by primary antibody omission. Sections were washed 3 times for 10 minutes with PBS and subsequently incubated with horseradish peroxidise–labeled α-mouse/rabbit secondary antibody (Dako REAL EnVision/HRP Rabbit/Mouse, Dako). Color was developed using 3,3-diaminobenzidine (DAB; 0.1 mg/ml, 0.02% $H_2O_2$, 10 minutes; Sigma, St. Louis, MO) as chromogen. Sections were counterstained with hematoxylin and mounted using Depex (BDH laboratories Supplies, East Grinstead, UK).

**Table 2**
Cases used for immunohistochemical analysis

| Case patient | Clinical diagnosis | *MAPT* mutation | Age (y) | Sex | Cause of death | PMD (hrs:min) |
|---|---|---|---|---|---|---|
| 1 | PiD | – | 68 | F | Pneumonia | 6:46 |
| 2 | PiD | – | 57 | M | General deterioration | 6:40 |
| 3 | PiD | – | 70 | M | Pneumonia | 5:15 |
| 4 | PiD | – | 82 | M | Pneumonia | 4:10 |
| 5 | PSP | – | 75 | M | Unknown | 5:05 |
| 6 | PSP | – | 72 | F | Infection | 6:15 |
| 7 | PSP | – | 80 | M | Dehydration, uremia | 4:50 |
| 8 | PSP | – | 67 | M | Pneumonia | 6:45 |
| 9 | PiD | G272V | 54 | F | Cachexia and dehydration | 5:40 |
| 10 | PiD | G272V | 54 | F | Cardiac arrest | 7:30 |
| 11 | PiD | G272V | 67 | F | Cachexia and dehydration | 4:10 |
| 12 | FTD | G272V | 49 | M | Suffocation (unnatural death) | 5:10 |
| 13 | FTD | G272V | 51 | M | Pneumonia | 4:25 |
| 14 | PiD | P301L | 64 | F | Unknown | 5:10 |
| 15 | PiD | P301L | 66 | F | Cachexia and dehydration | 6:40 |
| 16 | PiD | P301L | 46 | M | Unknown | 5:35 |
| 17 | PiD | P301L | 66 | M | Pneumonia | 5:00 |
| 18 | CTRL | – | 66 | M | Abdominal aortic aneurysm | 7:45 |
| 19 | CTRL | – | 61 | F | Euthanasia | 6:50 |

Key: CTRL, control; F, female; FTD, frontotemporal dementia; GFM, gyrus frontalis medialis; HIP, hippocampus; M, male; MAPT, microtubule associated protein tau; PiD, Pick's disease; PMD, post mortem delay; PSP, progressive supranuclear palsy.

### 2.6. Double immunohistochemistry

#### 2.6.1. pPERK and GSK-3/pSer$^{21/9}$ GSK-3

After quenching endogenous peroxidase activity, sections were pre-incubated with normal swine serum (1:10 dilution) for 10 minutes and subsequently incubated with pPERK antibody for 60 minutes at RT. After washing, sections were incubated with biotin-conjugated swine anti-rabbit F(ab')2 (1:300 dilution) for 30 minutes at RT, washed and incubated with alkaline phosphatase-conjugated streptavidin (sAP, 1:100 dilution). Color was developed using Liquid Permanent Red (LPR; Dako) as chromogen. Sections were treated in 10 mmol/L, pH 6.0, sodium citrate buffer heated by autoclave for 10 minutes and incubated for 16 hours at 4 °C with mouse anti-GSK-3 or rabbit anti-pSer$^{21/9}$ GSK-3. After washing, sections were incubated with EnVision goat anti-mouse HRP or goat anti-rabbit HRP (undiluted, Dako) for 30 minutes at RT. Color was developed using DAB as chromogen.

#### 2.6.2. AT8 and GSK-3/pSer$^{21/9}$ GSK-3

Sections were preincubated with NGS (1:10 dilution) for 10 minutes, incubated with AT8 antibody for 60 minutes at RT, and after washing incubated with EnVision goat anti mouse HRP (undiluted; Dako) for 30 minutes at RT. Color was developed using DAB. After washing and treatment in 10 mmol/L sodium citrate buffer pH, 6.0, in the autoclave for 10 minutes, sections were pre-incubated with NGS (1:10 dilution) for 10 minutes and subsequently incubated with GSK-3 antibody for 16 hours at 4 °C. After washing, sections were incubated with sAP (1:100 dilution) for 60 minutes at RT, and color was developed using LPR.

For AT8 and pSer$^{21/9}$ GSK-3 double immunohistochemistry sections were treated as described above and subsequently incubated with a mix of AT8 and pSer$^{21/9}$ GSK-3 for 16 hours at 4 °C. Sections were washed in PBS and subsequently incubated with a mix of SwαR$^{BIO}$ (1:300 dilution) and GαMIgG1$^{HRP}$ (1:100 dilution) for 60 minutes at RT. Sections were washed and incubated with sAP (1:100 dilution) for 60 minutes at RT. Sections were developed using DAB, and subsequently using LPR.

#### 2.6.3. Cathepsin D and pSer$^{21/9}$ GSK-3

Endogenous peroxidise activity was quenched and sections were treated in 10 mmol/L sodium citrate buffer, pH6.0, in a microwave for 10 minutes. Sections were preincubated with NGS (1:10 dilution) for 10 minutes at RT and subsequently incubated with a mix of cathepsin D and pSer$^{21/9}$ GSK-3 for 16 hours at 4 °C. After washing, sections were incubated with SwαR$^{BIO}$ (1:300 dilution) and Envision goat anti mouse HRP (undiluted, Dako) for 60 minutes at RT. Sections were washed and incubated with sAP (1:100 dilution) for 60 minutes at RT. Sections were developed using DAB, and subsequently developed using LPR.

For all double stainings, nuclei were stained with hematoxylin, and sections were mounted using Aquamount (BDH Laboratories Supplies, Radnor, PA). Cross-reactivity controls were generated by omission of primary antibodies. The Nuance spectral imaging system (Cri; Woburn, MA) was used to analyze the double-stained sections (Nijholt et al., 2011c). Spectral libraries of single-brown (DAB), single-red (LPR), and hematoxylin were obtained from control sections. The spectral library was used to unmix the different reaction products in double-stained sections into black and white images. These images represent the localization of each reaction product, and were converted to fluorescent-like images composed of pseudo-colors by the Nuance software.

### 2.7. Immunocytochemistry

Paraformaldehyde (PFA), 4% in PBS, was added to the medium in the well for 5 minutes at RT to obtain a 2% PFA solution for pre-fixation. Subsequently, cells were fixed with 4% PFA in PBS for 10 minutes. All washing steps were performed with PBS and repeated 3 times. Antibodies were diluted in 5% (w/v) BSA fraction V (Roche Diagnostics, Mannheim, Germany) in PBS. Cells were washed and blocked for 30 minutes at RT with 5% BSA in PBS containing 0.5% (v/v) Triton for cell permeabilization and incubated with the LAMP1 antibody for 2 h at RT. After washing, anti-rat secondary antibody (Jackson ImmunoResearch, West Grove, PA) was applied for 1 hour at RT. Cells were washed and incubated with GSK-3 antibody overnight at 4 °C. Washing was followed by incubation of the anti-rabbit secondary antibody (Jackson ImmunoResearch) in a dark chamber for 1 hour. Cells were washed before incubation with 4′,6-diamidino-2-phenylindole (DAPI) for 5 minutes. After a final washing step, cells were mounted with Prolong Gold Antifade Reagent (Invitrogen).

## 3. Results

### 3.1. UPR activation decreases total and pSer$^{21/9}$ GSK3 levels and increases GSK-3 activity in vitro

We investigated the effect of UPR activation on the phosphorylation status of GSK-3 in vitro. An InCell ELISA colorimetric assay, combined with GSK-3 and phosphorylated GSK-3 specific antibodies, was used to investigate GSK-3 in differentiated SK-N-SH neuroblastoma cells. The different (phospho) specific antibodies used in this study do not distinguish the paralogous proteins GSK-3α and GSK-3β. Cells were treated with tunicamycin (Tm) to chemically induce the UPR. Tm inhibits N-linked glycosylation, leading to the accumulation of proteins in the ER and subsequent activation of the UPR. Wm and lithium chloride (LiCl) were used as controls for stimulation and inhibition of GSK-3 activity, respectively. When pSer$^{21/9}$ and pTyr$^{216/279}$ GSK-3 are presented as a percentage of total GSK-3, Tm led to a decrease in pSer$^{21/9}$ (13%, 22%, and 16% reduction, $p < .01$) and an increase in pTyr$^{216/279}$ GSK (18%, 15% ($p < .01$) and 27% increase ($p < .05$), for 0.2, 0.5, and 1.0 μg/mL Tm, respectively), findings that are indicative of increased GSK-3 activity (Fig. 1A). In accordance with the literature, Wm resulted in 50% ($p < .01$) decrease (Grimes and Jope, 2001; Li et al., 2006) and LiCl in 15% ($p < .05$) increase (Chalecka-Franaszek and

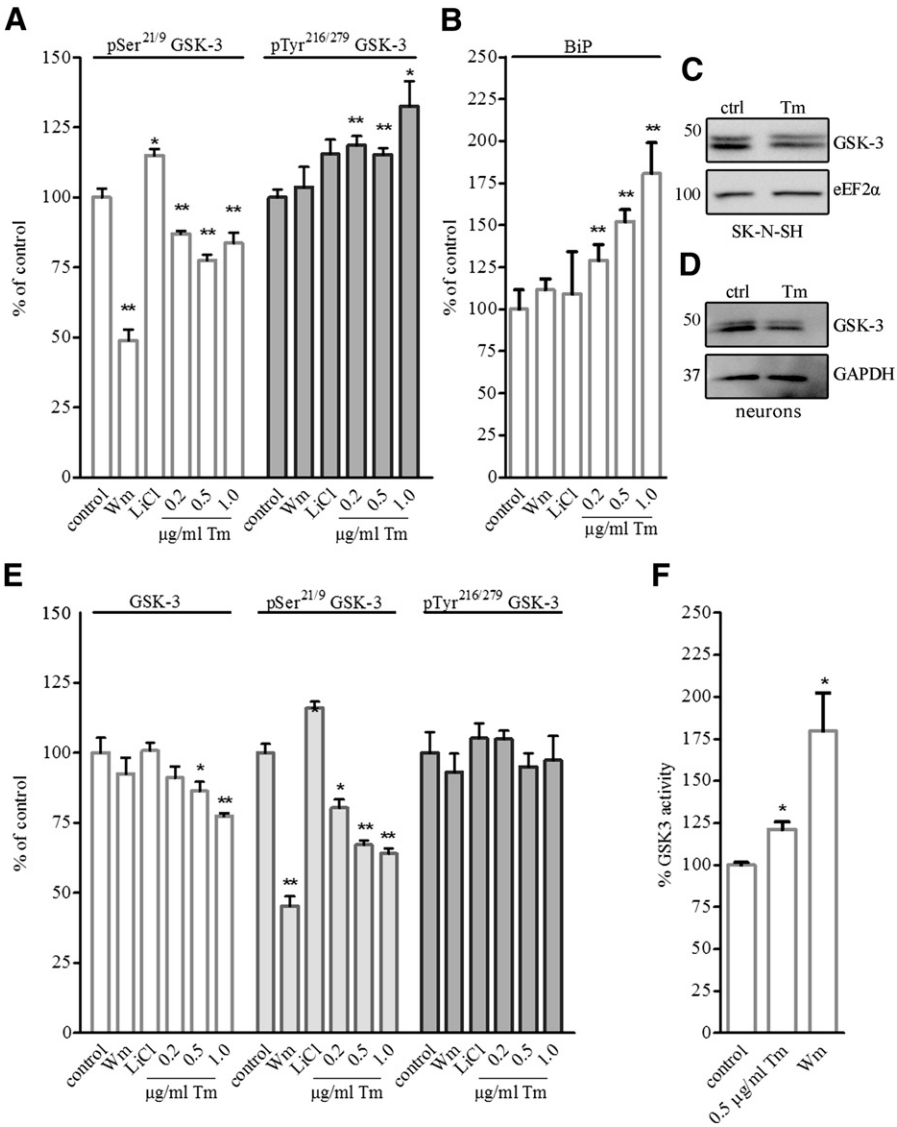


**Fig. 1.** UPR activation reduces pSer$^{21/9}$ GSK-3 levels and increases GSK-3 activity. Differentiated SK-N-SH cells were treated with increasing concentrations of Tm for 16h. Treatment with Wm and LiCl are indicated as positive and negative controls. Total and phosphorylated levels of GSK-3 and the ER chaperone BiP were investigated using an InCell ELISA colorimetric assay. One representative experiment for the InCell ELISA assay is shown; all measurements were performed in triplicate and each experiment was performed at least 3 times. (A) pSer$^{21/9}$ and pTyr$^{216/279}$ are expressed as a percentage of total GSK-3. Untreated cells are set to 100%. (B) Levels of BiP increased after treatment with Tm, indicating that the UPR is active under these conditions. (C) Differentiated SK-N-SH cells were incubated for 16 hours with (Tm) or without (crtl) 1 µg/mL Tm and (D) mouse primary neurons were treated for 16 hours with or without 5 µg/mL Tm. Equal amounts of cell extracts were analysed by Western blotting using antibodies as stated, eEF2α, and GAPDH were used as loading control. (E) Total GSK-3, pSer$^{21/9}$ GSK-3, and pTyr$^{216/279}$ GSK-3 levels corrected for the amount of cells by Janus Green staining. Values in untreated cells are set to 100%. (F) GSK-3 activity was determined by measuring the incorporation of radioactive phosphate on a GSK-3 specific substrate peptide in lysates of SK-N-SH cells treated with Tm and Wm. Bars represent the mean ± SEM of 2 independent experiments. $^{*}p < .05$, $^{**}p < .01$.

Chuang, 1999) of pSer$^{21/9}$ GSK-3, consistent with stimulation and inhibition of GSK-3 activity, respectively (Fig. 1A). Both Wm and LiCl did not affect pTyr$^{216/279}$ GSK-3 levels. Levels of the UPR target BiP increased after Tm treatment (29%, 52%, and 81% increase ($p < .05$) for 0.2, 0.5, and 1.0 µg/mL Tm, respectively), indicating that the UPR is also activated in a dose-dependent manner under these conditions (Fig. 1B). At a concentration of 0.1 µg/mL Tm, we found no UPR activation (not shown), therefore the lowest concentration used in our experiments was 0.2 µg/mL. As expected, neither Wm nor LiCl led to increased BiP levels.

The observed changes can be caused by a direct effect on phosphorylation or a change in GSK-3 levels. Therefore, the total GSK-3 level was determined after Tm treatment on Western blot and showed a decrease in the total levels (Fig. 1C). This Tm-induced decrease in total levels of GSK-3 is also found in mouse primary neurons (Fig. 1D), indicating that this is not merely a specific feature of neuroblastoma cells (a higher Tm concentration was used in the primary neurons to elicit a comparable UPR response, data not shown). To investigate whether the GSK-3 phosphoforms are differentially affected by Tm treatment, the data from the InCell ELISA were represented relative to the number of cells. Tm treatment led to a decrease in pSer$^{21/9}$ GSK-3 levels (20% ($p < .05$), 33%, and 36% ($p < 0.01$) reduction for 0.2, 0.5, and 1.0 µg/mL Tm, respectively), whereas pTyr$^{216/279}$ GSK-3 levels did not change (Fig. 1E). Interestingly, treatment with Tm also caused a dose-dependent decrease in total GSK-3 levels that reached statistical significance for 0.5 µg/mL Tm (14% reduction, $p < .05$) and 1.0 µg/mL Tm (23% reduction ($p < .01$). This is corroborated by quantification of total GSK-3 corrected for eEF2α after treatment with 1.0 µg/mL Tm on Western blot (Fig. 1C; reduction 23% ± 0.10, n = 4 from

separate experiments). In summary, activation of the UPR with Tm results in decreased levels of total and pSer$^{21/9}$ GSK-3 in a dose-dependent manner, where, at the highest concentration used, both the UPR response and the effect at the total and pSer$^{21/9}$ GSK-3 levels are most pronounced. Interestingly, we did not observe any significant changes in total GSK-3 levels after treatment with LiCl or Wm, which are known to act on pSer$^{21/9}$ phosphorylation itself, suggesting that the UPR operates via a different mechanism.

Next we investigated whether the Tm-induced changes in the relative amounts of pSer$^{21/9}$ and pTyr$^{216/279}$ GSK-3 have an actual effect on protein kinase activity. The activity of GSK-3 was measured using an assay described by Ryves et al. (Ryves et al., 1998). With this method, GSK-3 activity can be measured in crude cell extracts. In short, the transfer of $\gamma$-$^{32}$P from [$\gamma$-$^{32}$P] ATP to a GSK-3–specific primed substrate peptide was measured using scintillation counting. Each sample was assayed in the presence and absence of LiCl, and the difference between these values was used as a measure of GSK-3 activity. As expected, Wm resulted in an increase in GSK-3 activity (80% increase; $p < .05$), indicating we can measure changes in activity in this setup. Also Tm resulted in a significant and consistent increase in GSK-3 activity 21% increase, ($p < .05$; Fig. 1F). These data are in accordance with the changes in phosphorylation in GSK-3 after Tm treatment, and confirm that UPR activation leads to an increase in GSK-3 activity.

### 3.2. GSK-3 immunoreactive granules are present in hippocampal neurons of tauopathy cases

Our in vitro data suggest a connection between UPR activation and GSK-3 protein levels and protein kinase activity. We have previously demonstrated that UPR activation occurs in AD and in non-AD tauopathies in close relation to tau pathology (Hoozemans et al., 2005; Hoozemans et al., 2009; Nijholt et al., 2011c). Therefore, we investigated the expression of GSK-3 and its phosphorylation status in the hippocampus of different tauopathies (Table 2). These cases are clinically diagnosed with PiD, PSP, or FTD, and are histopathologically classified as frontotemporal lobar degeneration with tau positive inclusions (FTLD-tau). The hippocampi of these FTLD-tau cases showed extensive tau pathology and UPR activation (Nijholt et al., 2011c), making it a suitable region to investigate the connection among UPR activation, tau phosphorylation, and GSK-3.

In all investigated cases, including non-demented controls, we observed diffuse GSK-3 immunoreactivity in the soma and axons of the hippocampal neurons. Little to no reactivity was evident in the surrounding neuropil or in non-neuronal cells (Fig. 2A and B). In addition, small but intensely stained GSK-3 immunoreactive granules were present in hippocampal neurons of all (both sporadic and *MAPT* associated) tauopathy cases (Fig. 2C and D). We investigated the phosphorylation status of GSK-3 using phospo-specific GSK-3 antibodies. The pSer$^{21/9}$ GSK-3 antibody showed little pSer$^{21/9}$ GSK-3 immunoreactivity in the soma or axons of hippocampal neurons, but revealed intensely stained immunoreactive granules in the tauopathy cases similar to those observed with the pan GSK-3 antibody (Fig. 2E–G). Immunohistochemical staining for pTyr$^{216/279}$ GSK-3 revealed a punctate staining pattern, and we observed no differences between control and tauopathy cases (data not shown). Combined, our data show that granules consisting of inactive, Ser$^{21/9}$ phosphorylated, GSK-3 are present in the hippocampal neurons of tauopathy cases and are not present in non-neurological controls.

### 3.3. GSK-3 immunoreactive granules occur in neurons that have activated the UPR and early tau pathology

To more precisely investigate the connection between UPR activation and GSK-3 immunoreactive granules, we performed double immunohistochemistry on a subset of our cohort (cases 2, 4, 10, and 15). Phosphorylated (p) PERK was used as a marker of an active UPR and was combined with antibodies directed against GSK-3 (Fig. 3A–C) and pSer$^{21/9}$ GSK-3 (Fig. 3D and E). In all investigated cases, pPERK and GSK-3 or pSer$^{21/9}$ GSK-3 immunoreactive granules co-occurred in the same neurons. No direct colocalization between pPERK and (pSer$^{21/9}$) GSK-3 was observed. Quantification of the number of pPERK positive neurons that contain GSK-3 granules in a subset of patients showed a range of approximately 20% to 60% per microscopic field with an average of 34% to 45% for the whole hippocampus (supplementary Table 1). We have previously demonstrated that UPR activation occurs in neurons in the brain of AD (Hoozemans et al., 2009) and FTLD-tau (Nijholt et al., 2011c) that contain phosphorylated tau that is not in densely aggregated form. In Figure 4, we show that neurons with prebody tau pathology contain (pSer$^{21/9}$) GSK-3 immunoreactive granules (Fig. 4A–D), whereas granules were not observed in neurons lacking tau pathology (Fig. 4A, C, and E).

Thus, the findings that pSer$^{21/9}$ GSK-3 granules accumulate in neurons with an active UPR and phosphorylated tau suggests a functional connection among UPR activation, GSK-3, and tau phosphorylation.

### 3.4. pSer$^{21/9}$ GSK-3 immunoreactive granules are positive for the lysosomal protease cathepsin D

We have recently shown that UPR activation leads to the preferential activation of the autophagy/lysosomal route to degrade accumulated proteins (Nijholt et al., 2011c). Our in vitro data show that levels of inactive pSer$^{21/9}$ GSK-3 decrease after UPR activation, whereas we find accumulation of pSer$^{21/9}$ GSK-3 in granules in UPR positive neurons in tauopathies. This led us to hypothesize that, during an active UPR, part of the GSK-3 pool is selectively degraded by the lysosomal pathway.

To investigate whether UPR activation targets GSK-3 to the lysosomal compartment, we studied the localization of GSK-3 in differentiated SK-N-SH cells as well as in mouse primary neurons. In both cell types, GSK-3 is abundant and diffusely distributed throughout the cells (Fig. 5). Confocal analysis of double immunofluorescence staining with the lysosomal membrane protein LAMP1 was performed. The LAMP1-positive structures are in the SK-N-SH more confined to a juxtanuclear site, whereas in the neurons they are distributed throughout the soma. In both cell types, we observe co-localization of GSK-3 with lysosomes, supporting a role for the lysosomes in the degradation of GSK-3. However, in neither cell type is relocalization of GSK-3 observed upon Tm treatment (Fig. 5). This may be due to the high abundance of the GSK-3 throughout the cells, which makes it technically difficult to visualize a shift of a 20% sub-pool with this technique.

To further investigate whether the GSK-3 positive structures in tauopathies represents material targeted to lysosomes, we performed double immunohistochemistry on cases 2 and 15, using antibodies directed against the lysosomal protease cathepsin D and pSer$^{21/9}$ GSK-3. As expected, the cathepsin D antibody revealed a granular staining pattern, in accordance with its presence in lysosomes. A large fraction of pSer$^{21/9}$ GSK-3-positive granules were also cathepsin D positive (Fig. 6A–C). This indicates that, in tauopathies, pSer$^{21/9}$ GSK-3 is targeted to lysosomal structures in neurons with an active UPR.

### 3.5. UPR induces lysosomal degradation of GSK-3 in vitro

If the lysosomal route is indeed responsible for UPR-mediated degradation of GSK-3, then inhibition of lysosomal degradation during the UPR should rescue GSK-3 levels in vitro. To investigate

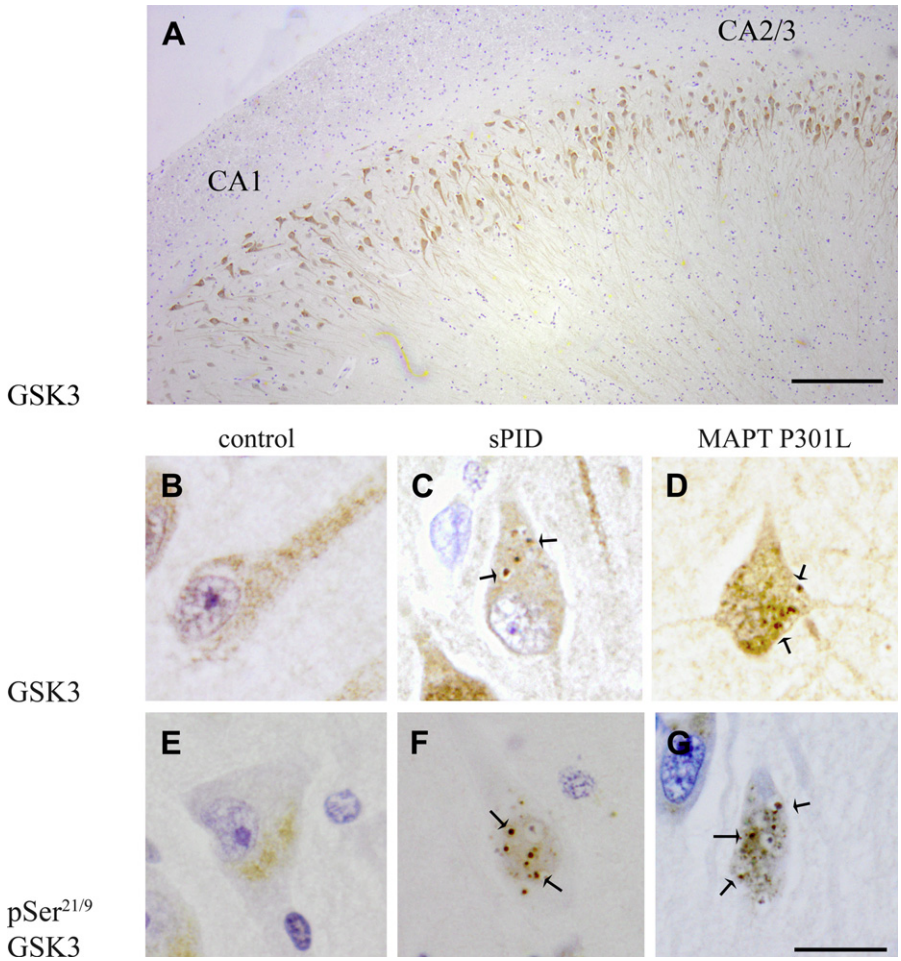


**Fig. 2.** GSK-3 and pSer$^{21/9}$ GSK-are localized in granules in hippocampal neurons in tauopathy cases. Immunohistochemistry was performed to evaluate the expression of GSK-3 and its phosphorylation status in tauopathies. (A) Expression of GSK-3 is apparent in the pyramidal neurons of the hippocampus (control case). (B–G) Higher-magnification images are shown from a representative control, sporadic PiD, and a *MAPT* mutation carrier assayed for the presence of total GSK-3 (B–D) and pSer$^{21/9}$ GSK-3 (E–G). Intensely stained granules were visible with the GSK-3 and pSer$^{21/9}$ GSK-3 antibodies in tauopathy cases. Nuclei were counterstained using hematoxylin. Arrows indicate GSK-3 immunoreactive granules. Scale bars, 200 and 50 μm.

this, differentiated SK-N-SH cells were treated with Tm in the presence or absence of BAF. This compound inhibits lysosomal degradation by inhibiting the vacuolar-type ATPase and increasing the pH of lysosomal vesicles (Bowman et al., 1988; Drose et al., 1993). Levels of GSK-3 were assayed using the InCell ELISA colorimetric assay. As shown before, induction of the UPR led to a significant decrease in total GSK-3 levels. Co-treatment of Tm with BAF rescued the Tm induced degradation of GSK-3, whereas no effect was observed on pTyr$^{216/279}$ levels (Fig. 7A). This suggests that a pTyr$^{216/279}$ negative subset of GSK-3 is targeted for lysosomal degradation during UPR activation. Based on our other data, we suggest that pSer$^{21/9}$ GSK-3 is a likely candidate for this selective degradation by the lysosomes. We were unable to obtain informative results with pSer$^{21/9}$ GSK-3, because treatment with BAF alone decreased the level of pSer$^{21/9}$ GSK-3 (Fig. 7A).

To verify that pSer$^{21/9}$ GSK-3 is indeed a substrate for lysosomal degradation, the activity of the autophagy/lysosomal pathway was induced in SK-N-SH cells by amino acid deprivation (Mortimore et al., 1989; Susan and Dunn, 2001) for 2 hours. Levels of GSK-3, pSer$^{21/9}$, and pTyr$^{216/279}$ GSK-3 were assayed. Amino acid deprivation led to a decrease in GSK-3 and pSer$^{21/9}$ GSK-3 levels (Fig. 7B), but had no effect on pTyr$^{216/279}$ levels. This indicates that pSer$^{21/9}$ but not pTyr$^{216/279}$ GSK-3 is a substrate for autophagy and is degraded in the lysosomes.

## 4. Discussion

In this study, we have identified a specific mechanism for activation of GSK-3 via the UPR, which may explain the close association of the UPR and early stages of tau pathology. UPR activation in an in vitro cell model led to a decrease in the levels of total and inactive Ser$^{21/9}$ phosphorylated GSK-3, resulting in a relative increase in active Tyr$^{216/279}$ phosphorylated GSK-3 and increased protein kinase activity. Increased activity of GSK-3 by UPR activation was previously observed (Fu et al., 2010; Song et al., 2002), but the mechanism has remained elusive. In the current study, we provide evidence that UPR-mediated activation of the tau kinase GSK-3 occurs via the lysosomal degradation of inactive GSK-3. This is compatible with the pSer$^{21/9}$GSK-3 functioning as a dominant negative, as has been shown for catalytically inactive GSK-3 (Dominguez et al., 1995). Regulation of total and pSer$^{21/9}$GSK-3 by lysosomal degradation has been shown in primary cardiac myocytes. In this study, overexpression of the lysosomal protease cathepsin L decreased the amount of inactive pSer$^{21/9}$ GSK-3, whereas knockdown enhanced the level of pSer$^{21/9}$ GSK-3 (Tang et al., 2009). Both the classical GSK-3 activator Wm and the widely used inhibitor LiCl affect the level of pSer$^{21/9}$ GSK-3 directly via phosphorylation. This mechanism is different from the UPR-mediated regulation, because the GSK-3 protein levels are not affected.

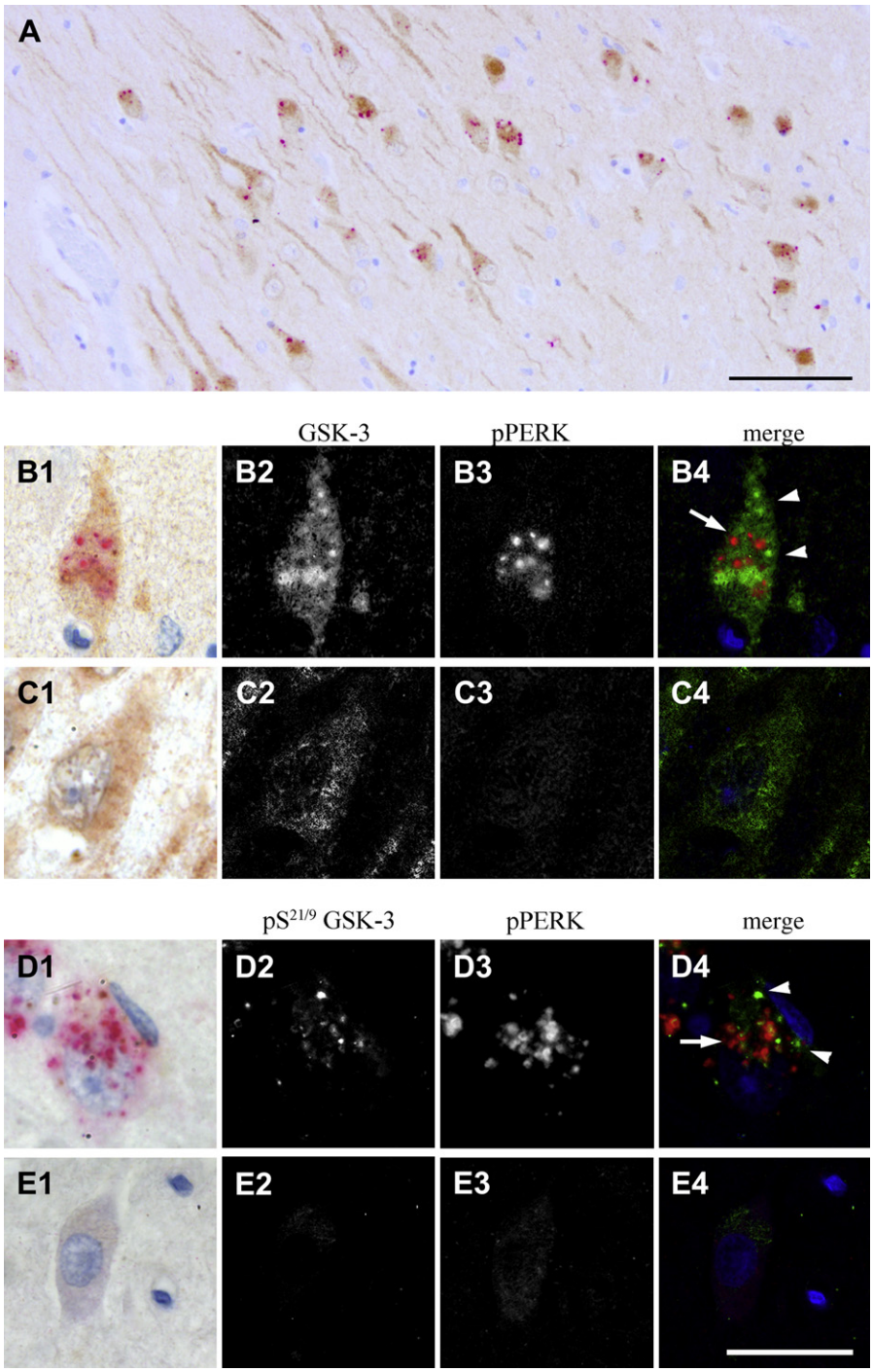


**Fig. 3.** GSK-3 immunoreactive granules occur in neurons that have an activated UPR. Double immunohistochemistry was performed on a subset of our cohort using GSK-3/pSer$^{21/9}$ GSK-3 and pPERK antibodies. (A) Low-magnification area of the CA1 region of a sporadic PiD case (#2) stained with GSK-3 (brown) and pPERK (pink) is shown. Nuclei were counterstained with hematoxylin (blue). (B and C) Spectral imaging was performed on higher magnification images (B1, C1) to unmix the different chromogens and GSK-3 (B2, C2) and pPERK (B3, C3) are shown separately and as a merge with artificial colors (GSK-3, green; pPERK, red; B4, C4). (D and E) The same approach was used for pSer$^{21/9}$ GSK-3 (brown) and pPERK (pink) double immunohistochemical stainings (D1, E1). Spectral imaging was performed; pSer$^{21/9}$ GSK-3 (D2, E2) and pPERK (D3, E3) are shown separately and as a merge with artificial colors (pSer$^{21/9}$ GSK-3, green; pPERK, red; D4, E4). Representative neurons that contain (pSer$^{21/9}$) GSK-3 reactive granules and pPERK (B and D) are shown. Neurons lacking pPERK also do not contain (pSer$^{21/9}$) GSK-3 reactive granules (C and E). Arrows indicate pPERK reactive granules, arrowheads indicate (pSer$^{21/9}$) GSK-3 reactive granules. Scale bars, 50 and 25 μm.

In tauopathies, the inactive, Ser$^{21/9}$-phosphorylated form of GSK-3 was found to accumulate in granules in hippocampal neurons. GSK-3 immunoreactive granules were previously observed in hippocampal neurons in AD brain (Hoozemans et al., 2009; Leroy et al., 2002). The presence of Aβ in the AD brain may complicate the analysis of the connection between GSK-3 and the UPR, as Aβ was shown to increase GSK-3 activity (Takashima et al., 1998) and to sensitize cells for UPR activation (Chafekar et al., 2007; Chafekar et al., 2008). In our cohort of non-AD tauopathies, Aβ pathology was only rarely observed (Nijholt et al., 2011c), allowing

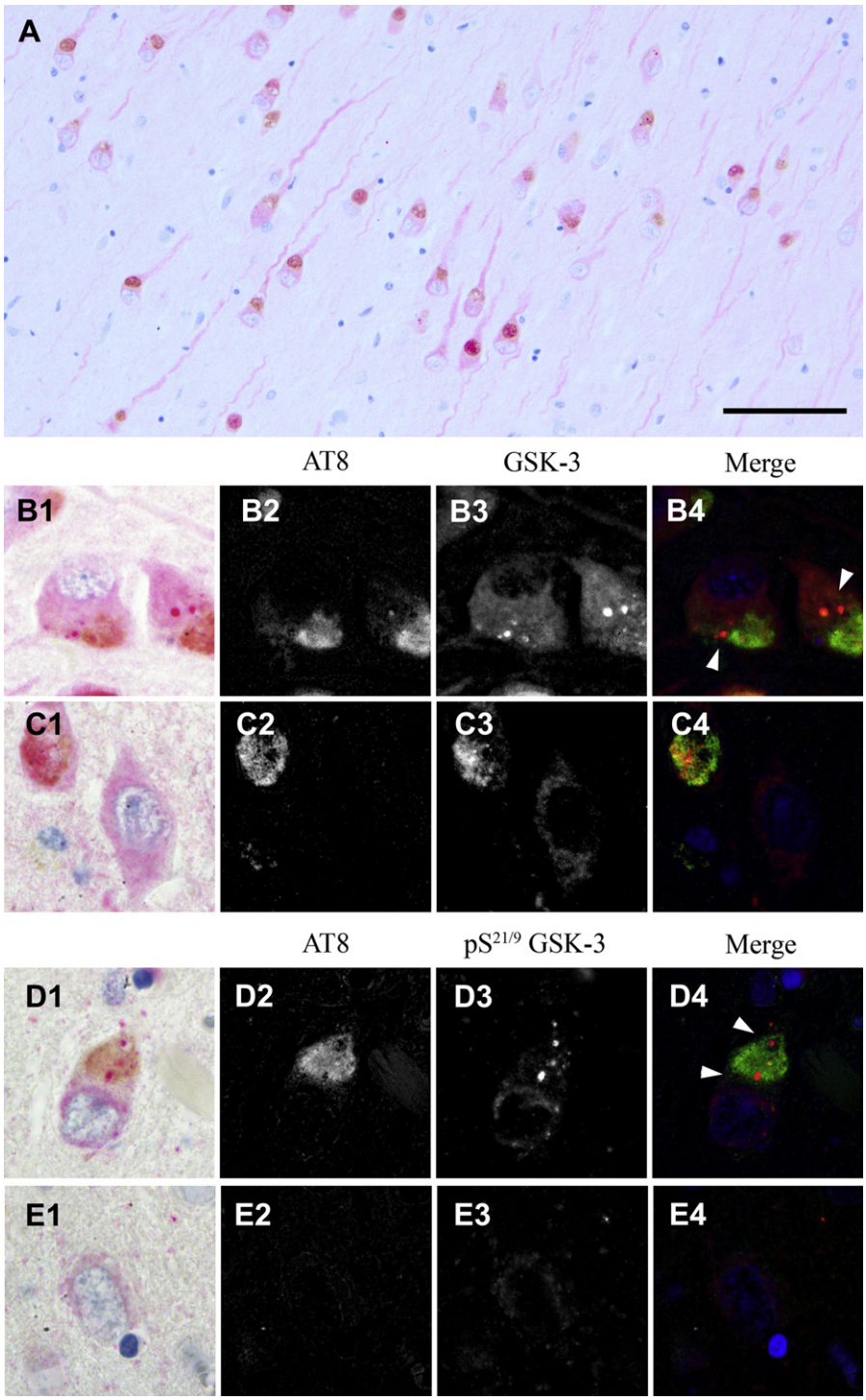


**Fig. 4.** GSK-3 reactive granules occur in neurons that contain phosphorylated tau pathology. Double immunohistochemistry was performed on a subset of our cohort using AT8 (p-tau) and GSK-3/pSer$^{21/9}$ GSK-3 antibodies. (A) Shown is a low magnification area of the CA1 region of a sporadic PiD case (#2) stained with AT8 (brown) and GSK-3 (pink). Nuclei were counterstained with hematoxylin (blue). Spectral imaging was performed on higher-magnification images (B1, C1) to unmix the different chromogens; AT8 (B2, C2) and GSK-3 (B3, C3) are shown separately and as a merge with artificial colors (AT8, green; GSK-3, red, B4, C4). The same approach was used for AT8 and pSer$^{21/9}$ GSK-3 double immunohistochemical stainings (E1, D1). Spectral imaging was performed; AT8 (D2, E2) and pSer$^{21/9}$ GSK-3 (D3, E3) are shown separately and as a merge with artificial colors (AT8, green; pSer$^{21/9}$ GSK-3, red, D4, E4). Representative neurons that contain (pSer$^{21/9}$) GSK-3 reactive granules and p-tau pathology (B and D) are shown. Neurons without AT8 positivity also do not contain (pSer$^{21/9}$) GSK-3 reactive granules (C and E). Arrowheads indicate (pSer$^{21/9}$) GSK-3 reactive granules. Scale bar, 50 μm.

study of the connection between UPR activation and GSK-3 without confounding effects of Aβ. Double immunohistochemistry revealed pSer$^{21/9}$ GSK-3 immunoreactive granules to occur in neurons of the tauopathy brain that had activated the UPR (Nijholt et al., 2011c). We previously demonstrated that in the AD and FTLD-tau brain, UPR activation occurs in neurons that contain diffusely distributed p-tau. Our observations in this study further strengthen the connection between UPR activation, GSK-3, and tau phosphorylation. pPERK and other UPR markers are commonly observed in granules with a distinct morphological profile, referred to as

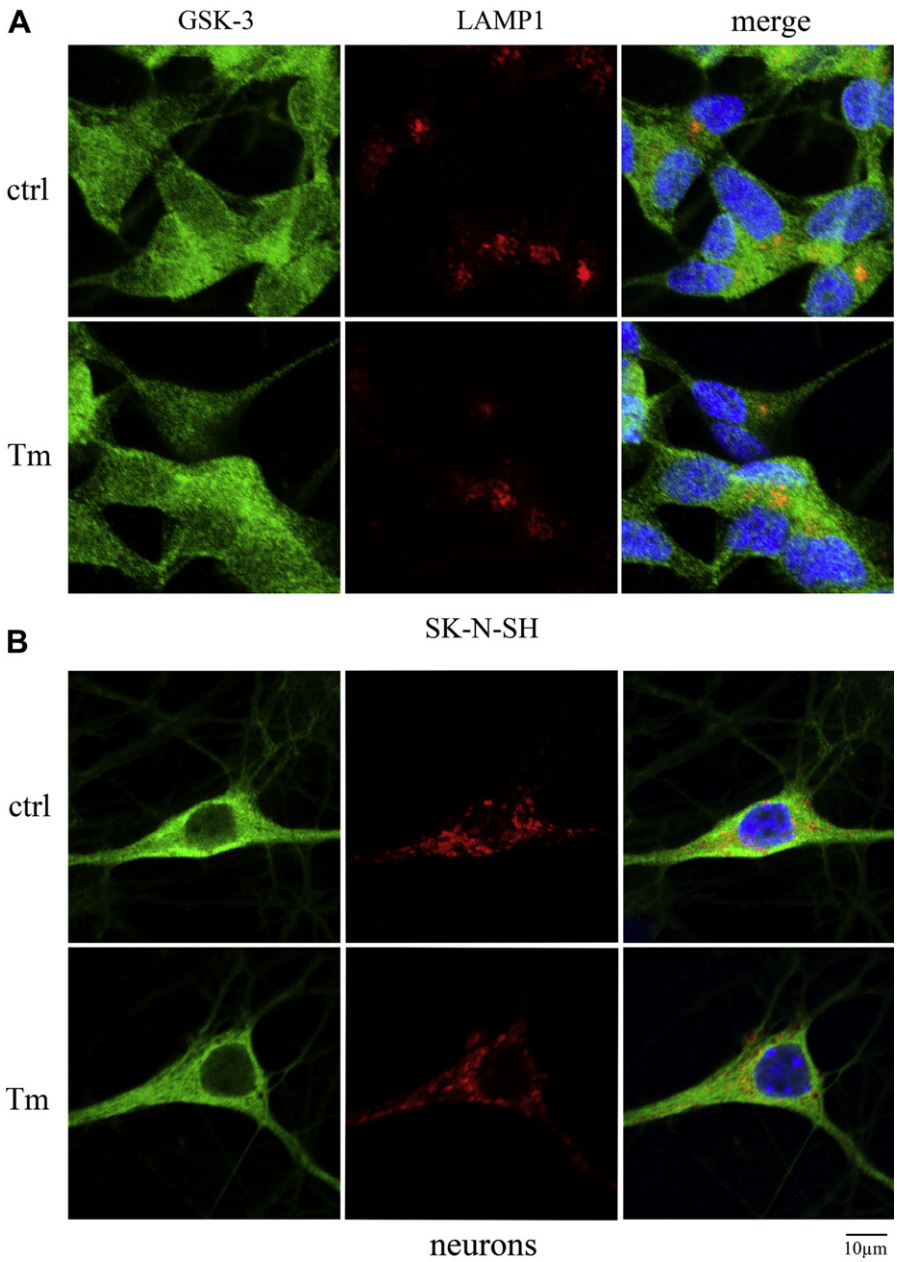


**Fig. 5.** GSK-3 co-localizes with the lysosomal marker LAMP1. (A) Differentiated SK-N-SH cells and (B) mouse primary neurons were incubated for 16 hours with (Tm) or without (ctrl) 1 and 5 μg/mL tunicamycin, respectively, to activate the UPR. Immunofluorescent analyses were performed using GSK3β antibody and LAMP1 antibody as lysosomal marker. Nuclei were counterstained with DAPI. GSK-3 localization was assessed by confocal microsopy. One representative image is shown for each condition.

granulovacuolar degeneration (Hoozemans et al., 2009; Nijholt et al., 2011c). We observed no direct colocalization of pPERK and pSer$^{21/9}$ GSK-3 reactive granules. Instead, a large fraction of pSer$^{21/9}$, GSK-3 was found to colocalize with cathepsin D immunoreactive lysosomal structures, suggesting that inactive GSK-3 is targeted to the lysosomes. In both SK-N-SH cells as well as in mouse primary neurons, GSK-3 co-localizes with LAMP1 positive structures. This is corroborated by in vitro data that show that inhibition of lysosomal degradation prevents the UPR-induced decrease in GSK-3 levels. In this experiment, we were unable to obtain informative results for the degradation of pSer$^{21/9}$ GSK-3, because treatment with BAF alone decreased the level of pSer$^{21/9}$ GSK-3. Stimulation of lysosomal degradation by amino acid starvation does induce a selective decrease in pSer$^{21/9}$ GSK-3, therefore the effect of BAF is probably indirect. BAF was shown to induce changes in the phosphorylation of insulin receptor signaling components, including PKB/Akt, which targets GSK-3 Ser$^{21/9}$ (Hettiarachchi et al., 2006). Thus, the decrease in pSer$^{21/9}$ GSK-3 levels that we observe might be caused by BAF acting on upstream components of the insulin signaling pathway. Starvation activates the autophagy/lysosomal route by inhibiting mTOR, the major regulator of autophagy induction. There are multiple signaling pathways that interconnect mTORC complexes, the UPR and GSK-3, that are not yet fully understood (Appenzeller-Herzog and Hall, 2012). However, we observe that starvation affects the total levels of GSK-3 and not the phosphorylation status, indicating that it is mediated via autophagy/lysosomal degradation and does not involve signaling via kinases that target GSK-3 Ser$^{21/9}$.

In our cell model, pTyr$^{216/279}$ GSK is apparently not subject to UPR induced degradation. In addition, in post-mortem tissue, the localization of this phosphorylated isoform is not changed in

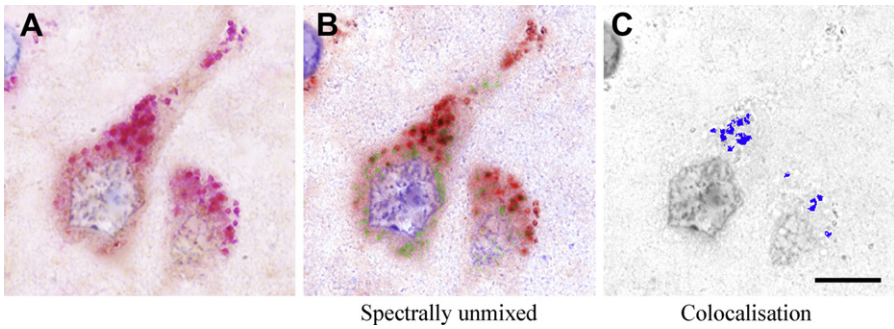


**Fig. 6.** pSer$^{21/9}$ GSK-3 granules co-localize with the lysosomal marker cathepsin D. Double immunohistochemistry was performed on a subset of our cohort. (A) High-magnification image of the hippocampal CA1 region of a sporadic PiD case (#2) stained with pSer$^{21/9}$ GSK-3 (brown) and cathepsin D (pink). Nuclei were counterstained with hematoxylin (blue). (B) Spectral imaging was performed to unmix the different chromogens and to assign artificial colors (pSer$^{21/9}$ GSK-3: green, cathepsin-D: red). (C) Colocalization between pSer$^{21/9}$ GSK-3 and cathepsin D is shown in blue. Scale bar, 10 μm.

tauopathies compared to control cases. We cannot exclude also that some GSK-3 that is not phosphorylated at pSer$^{21/9}$ is degraded. However, the strongest UPR-induced decrease is in the fraction that is phosphorylated at pSer$^{21/9}$, suggesting that this phosphorylated isoform is specifically targeted for degradation. UPR activation leads to increased autophagy (Yorimitsu et al., 2006), which would be a possible pathway to direct material for lysosomal degradation. We previously reported that, during UPR activation, the autophagy/lysosomal pathway is the preferred pathway for degradation (Nijholt et al., 2011a). Induction of autophagy by starvation also leads to a reduction in total and pSer$^{21/9}$ GSK-3, indicating that GSK-3 is a substrate macro autophagy. Alternatively, lysosomal targeting of pSer$^{21/9}$ GSK-3 may be achieved by fusion of a granule with a lysosome, or pSer$^{21/9}$ GSK-3 may be actively recruited to the lysosomes via a mechanism like chaperone-mediated autophagy. Autophagy is a dynamic process of which the activity is difficult to assess in situ (Klionsky et al., 2012). In our previous work, we observed high levels of LC3 in neurons that had activated the UPR in AD hippocampus, which is indicative of disturbed autophagic flux (Nijholt et al., 2011a). This may be caused by impaired lysosomal function, which is a well-established feature of AD (Boland et al., 2008; Lee et al., 2010; Lee et al., 2011; Nijholt et al., 2011b; Nixon et al., 2005). The accumulation of pSer$^{21/9}$ GSK-3 may reflect the recruitment of pSer$^{21/9}$ GSK-3 into lysosomal compartments that are not efficiently cleared because of an underlying defect in lysosomal degradation. Our activity data indicate that the inhibitory phosphorylation of GSK-3 at Ser$^{21/9}$, at least to some extent, functions as a dominant negative. This would imply that also in the absence of actual degradation, the sequestration of pSer$^{21/9}$ GSK-3 into the lysosomal compartment is expected to increase GSK-3 activity and promote tau phosphorylation. Interestingly, in a recent report, conditional and neuron-specific knockout mice for *Atg7*, a key player in autophagy, displayed inclusions of phosphorylated tau and GSK-3. This apparently is a very selective effect, as other proteins associated with neurodegenerative disorders like α-synuclein and APP/Aβ, or other tau kinases like CDK5 or GSK-3 substrates like β-catenin do not accumulate in these autophagy-deficient neurons (Inoue et al., 2012). This supports an important role of the autophagy/lysosomal system in the selective regulation of the activity of GSK-3 and the resulting phosphorylation of its substrate tau.

In summary, we have presented a novel mechanism by which the UPR increases activity of the major tau kinase GSK-3. When UPR

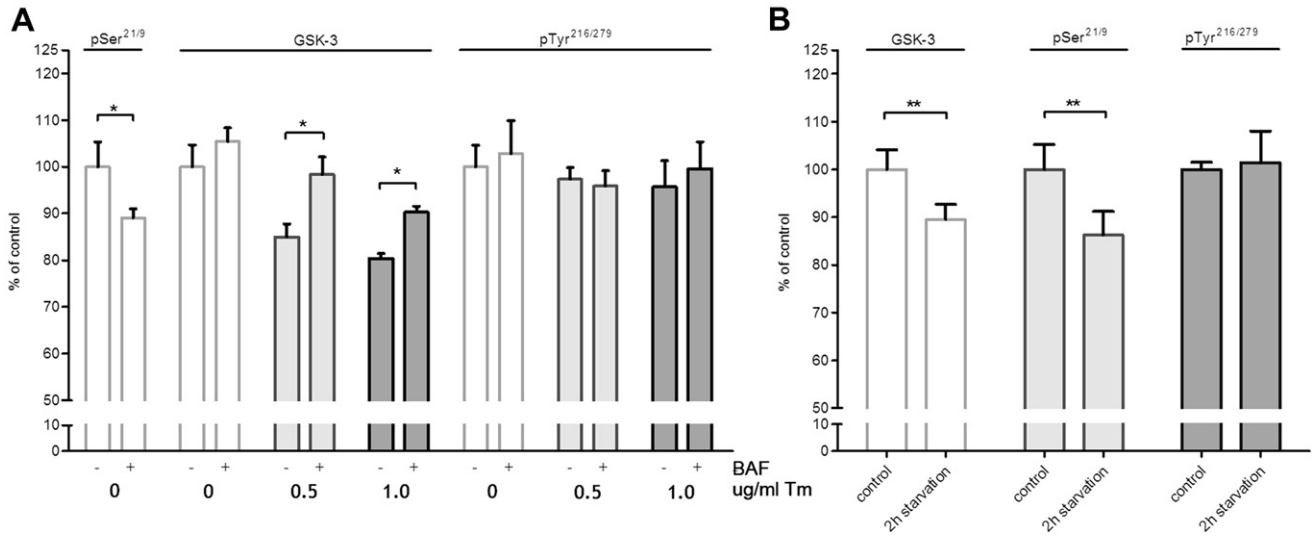


**Fig. 7.** UPR induces lysosomal degradation of GSK-3 in vitro. Levels of GSK-3 and pSer$^{21/9}$ and pTyr$^{216/279}$ GSK-3 were determined in differentiated SK-N-SH cells using the InCell ELISA colorimetric assay and corrected for cell number using Janus Green staining. Values in untreated cells are set to 100%. Bars represent the mean ± SEM of n = 3 from a representative experiment; all measurements were performed in triplicate, and each experiment was performed at least twice; $^{*}p < .05$, $^{**}p < .01$. (A) Cells were treated with increasing concentrations of Tm for 16 hours in the presence or absence of BAF to study the effect of inhibition of lysosomal degradation on the Tm induced decrease in GSK-3 levels. (B) To investigate whether the GSK-3 phosphoforms are specific substrates for autophagy/lysosomal degradation, cells were starved for 2 hours to induce autophagy.

activation persists, a prolonged increase in GSK-3 activity may disturb the balance between the activity of tau kinases and phosphatases in a way that favors increased tau phosphorylation and aggregate formation.

## Disclosure statement

The authors declare no actual and potential conflicts of interest.

## Acknowledgements

Human brain tissue was supplied by the Netherlands Brain Bank, Amsterdam, The Netherlands. This study was financially supported by Internationale Stichting Alzheimer Onderzoek (ISAO #7506) and Netherlands Organisation for Scientific Research (NWO). We thank Judith van der Harg, Hyung Elfrink and Line De Kimpe for stimulating discussions.

## Appendix. Supplementary data

Supplementary data associated with this article can be found, in the online version, at http://dx.doi.org/10.1016/j.neurobiolaging.2013.01.008.

## References

Alonso, A., Zaidi, T., Novak, M., Grundke-Iqbal, I., Iqbal, K., 2001. Hyperphosphorylation induces self-assembly of tau into tangles of paired helical filaments/straight filaments. Proc. Natl. Acad. Sci. U. S. A 98, 6923–6928.

Alonso, A.D., Di, C.J., Li, B., Corbo, C.P., Alaniz, M.E., Grundke-Iqbal, I., Iqbal, K., 2010. Phosphorylation of tau at Thr212, Thr231, and Ser262 combined causes neurodegeneration. J. Biol. Chem. 285, 30851–30860.

Appenzeller-Herzog, C., Hall, M.N., 2012. Bidirectional crosstalk between endoplasmic reticulum stress and mTOR signaling. Trends Cell Biol. 22, 274–282.

Ballatore, C., Lee, V.M., Trojanowski, J.Q., 2007. Tau-mediated neurodegeneration in Alzheimer's disease and related disorders. Nat. Rev. Neurosci. 8, 663–672.

Bancher, C., Brunner, C., Lassmann, H., Budka, H., Jellinger, K., Wiche, G., Seitelberger, F., Grundke-Iqbal, I., Iqbal, K., Wisniewski, H.M., 1989. Accumulation of abnormally phosphorylated tau precedes the formation of neurofibrillary tangles in Alzheimer's disease. Brain Res. 477, 90–99.

Bax, B., Carter, P.S., Lewis, C., Guy, A.R., Bridges, A., Tanner, R., Pettman, G., Mannix, C., Culbert, A.A., Brown, M.J., Smith, D.G., Reith, A.D., 2001. The structure of phosphorylated GSK-3beta complexed with a peptide, FRATtide, that inhibits beta-catenin phosphorylation. Structure 9, 1143–1152.

Boland, B., Kumar, A., Lee, S., Platt, F.M., Wegiel, J., Yu, W.H., Nixon, R.A., 2008. Autophagy induction and autophagosome clearance in neurons: relationship to autophagic pathology in Alzheimer's disease. J. Neurosci. 28, 6926–6937.

Bowman, E.J., Siebers, A., Altendorf, K., 1988. Bafilomycins: a class of inhibitors of membrane ATPases from microorganisms, animal cells, and plant cells. Proc. Natl. Acad. Sci. U. S. A 85, 7972–7976.

Brownlees, J., Irving, N.G., Brion, J.P., Gibb, B.J., Wagner, U., Woodgett, J., Miller, C.C., 1997. Tau phosphorylation in transgenic mice expressing glycogen synthase kinase-3beta transgenes. Neuroreport 8, 3251–3255.

Chafekar, S.M., Hoozemans, J.J., Zwart, R., Baas, F., Scheper, W., 2007. Abeta 1-42 induces mild endoplasmic reticulum stress in an aggregation state-dependent manner. Antioxid. Redox. Signal 9, 2245–2254.

Chafekar, S.M., Zwart, R., Veerhuis, R., Vanderstichele, H., Baas, F., Scheper, W., 2008. Increased Abeta1-42 production sensitizes neuroblastoma cells for ER stress toxicity. Curr. Alzheimer Res. 5, 469–474.

Chalecka-Franaszek, E., Chuang, D.M., 1999. Lithium activates the serine/threonine kinase Akt-1 and suppresses glutamate-induced inhibition of Akt-1 activity in neurons. Proc. Natl. Acad. Sci. U. S. A 96, 8745–8750.

Cho, J.H., Johnson, G.V., 2003. Glycogen synthase kinase 3beta phosphorylates tau at both primed and unprimed sites. Differential impact on microtubule binding. J. Biol. Chem. 278, 187–193.

Cowan, C.M., Bossing, T., Page, A., Shepherd, D., Mudher, A., 2010. Soluble hyperphosphorylated tau causes microtubule breakdown and functionally compromises normal tau in vivo. Acta Neuropathol. 120, 593–604.

Cuchillo-Ibanez, I., Seereeram, A., Byers, H.L., Leung, K.Y., Ward, M.A., Anderton, B.H., Hanger, D.P., 2008. Phosphorylation of tau regulates its axonal transport by controlling its binding to kinesin. FASEB J. 22, 3186–3195.

De Wit, J., Toonen, R.F., Verhage, M., 2009. Matrix-dependent local retention of secretory vesicle cargo in cortical neurons. J. Neurosci. 29, 23–37.

Dominguez, I., Itoh, K., Sokol, S.Y., 1995. Role of glycogen synthase kinase 3 beta as a negative regulator of dorsoventral axis formation in Xenopus embryos. Proc. Natl. Acad. Sci. U. S. A 92, 8498–8502.

Drose, S., Bindseil, K.U., Bowman, E.J., Siebers, A., Zeeck, A., Altendorf, K., 1993. Inhibitory effect of modified bafilomycins and concanamycins on P- and V-type adenosinetriphosphatases. Biochemistry 32, 3902–3906.

Fang, X., Yu, S.X., Lu, Y., Bast Jr., R.C., Woodgett, J.R., Mills, G.B., 2000. Phosphorylation and inactivation of glycogen synthase kinase 3 by protein kinase A. Proc. Natl. Acad. Sci. U. S. A 97, 11960–11965.

Fiol, C.J., Mahrenholz, A.M., Wang, Y., Roeske, R.W., Roach, P.J., 1987. Formation of protein kinase recognition sites by covalent modification of the substrate. Molecular mechanism for the synergistic action of casein kinase II and glycogen synthase kinase 3. J. Biol. Chem. 262, 14042–14048.

Forde, J.E., Dale, T.C., 2007. Glycogen synthase kinase 3: a key regulator of cellular fate. Cell Mol. Life Sci. 64, 1930–1944.

Fu, Z.Q., Yang, Y., Song, J., Jiang, Q., Liu, Z.C., Wang, Q., Zhu, L.Q., Wang, J.Z., Tian, Q., 2010. LiCl attenuates thapsigargin-induced tau hyperphosphorylation by inhibiting GSK-3beta in vivo and in vitro. J. Alzheimers. Dis. 21, 1107–1117.

Gendron, T.F., Petrucelli, L., 2009. The role of tau in neurodegeneration. Mol. Neurodegen. 4, 13.

Gomez-Sintes, R., Hernandez, F., Bortolozzi, A., Artigas, F., Avila, J., Zaratin, P., Gotteland, J.P., Lucas, J.J., 2007. Neuronal apoptosis and reversible motor deficit in dominant-negative GSK-3 conditional transgenic mice. EMBO J. 26, 2743–2754.

Grimes, C.A., Jope, R.S., 2001. The multifaceted roles of glycogen synthase kinase 3beta in cellular signaling. Prog. Neurobiol. 65, 391–426.

Hagen, T., Di, D.E., Culbert, A.A., Reith, A.D., 2002. Expression and characterization of GSK-3 mutants and their effect on beta-catenin phosphorylation in intact cells. J. Biol. Chem. 277, 23330–23335.

Hanger, D.P., Anderton, B.H., Noble, W., 2009. Tau phosphorylation: the therapeutic challenge for neurodegenerative disease. Trends Mol. Med. 15, 112–119.

Hanger, D.P., Hughes, K., Woodgett, J.R., Brion, J.P., Anderton, B.H., 1992. Glycogen synthase kinase-3 induces Alzheimer's disease-like phosphorylation of tau: generation of paired helical filament epitopes and neuronal localisation of the kinase. Neurosci. Lett. 147, 58–62.

Hanger, D.P., Noble, W., 2011. Functional implications of glycogen synthase kinase-3-mediated tau phosphorylation. Int. J. Alzheimers Dis. 2011, 352805.

Hartigan, J.A., Xiong, W.C., Johnson, G.V., 2001. Glycogen synthase kinase 3beta is tyrosine phosphorylated by PYK2. Biochem. Biophys. Res. Commun. 284, 485–489.

Hettiarachchi, K.D., Zimmet, P.Z., Myers, M.A., 2006. The plecomacrolide vacuolar-ATPase inhibitor bafilomycin, alters insulin signaling in MIN6 beta-cells. Cell Biol. Toxicol. 22, 169–181.

Hoglinger, G.U., Melhem, N.M., Dickson, D.W., Sleiman, P.M., Wang, L.S., Klei, L., Rademakers, R., de, S.R., Litvan, I., Riley, D.E., van Swieten, J.C., Heutink, P., Wszolek, Z.K., Uitti, R.J., Vandrovcova, J., Hurtig, H.I., Gross, R.G., Maetzler, W., Goldwurm, S., Tolosa, E., Borroni, B., Pastor, P., Cantwell, L.B., Han, M.R., Dillman, A., van der Brug, M.P., Gibbs, J.R., Cookson, M.R., Hernandez, D.G., Singleton, A.B., Farrer, M.J., Yu, C.E., Golbe, L.I., Revesz, T., Hardy, J., Lees, A.J., Devlin, B., Hakonarson, H., Muller, U., Schellenberg, G.D., 2011. Identification of common variants influencing risk of the tauopathy progressive supranuclear palsy. Nat. Genet. 43, 699–705.

Hoozemans, J.J.M., van Haastert, E.S., Nijholt, D.A.T., Rozemuller, A.J.M., Eikelenboom, P., Scheper, W., 2009. The unfolded protein response is activated in pretangle neurons in Alzheimer's disease hippocampus. Am. J. Pathol. 174, 1241–1251.

Hoozemans, J.J.M., Veerhuis, R., van Haastert, E.S., Rozemuller, J.M., Baas, F., Eikelenboorn, P., Scheper, W., 2005. The unfolded protein response is activated in Alzheimer's disease. Acta Neuropathol. 110, 165–172.

Inoue, K., Rispoli, J., Kaphzan, H., Klann, E., Chen, E.I., Kim, J., Komatsu, M., Abeliovich, A., 2012. Macroautophagy deficiency mediates age-dependent neurodegeneration through a phospho-tau pathway. Mol. Neurodegener. 7, 48.

Ishiguro, K., Shiratsuchi, A., Sato, S., Omori, A., Arioka, M., Kobayashi, S., Uchida, T., Imahori, K., 1993. Glycogen synthase kinase 3 beta is identical to tau protein kinase I generating several epitopes of paired helical filaments. FEBS Lett. 325, 167–172.

Ishiguro, K., Takamatsu, M., Tomizawa, K., Omori, A., Takahashi, M., Arioka, M., Uchida, T., Imahori, K., 1992. Tau protein kinase I converts normal tau protein into A68-like component of paired helical filaments. J Biol. Chem. 267, 10897–10901.

Klionsky, D.J., Abdalla, F.C., Abeliovich, H., Abraham, R.T., Acevedo-Arozena, A., Adeli, K., Agholme, L., Agnello, M., Agostinis, P., Aguirre-Ghiso, J.A., Ahn, H.J., Ait-Mohamed, O., Ait-Si-Ali, S., Akematsu, T., Akira, S., Al-Younes, H.M., Al-Zeer, M.A., Albert, M.L., Albin, R.L., Alegre-Abarrategui, J., Aleo, M.F., Alirezaei, M., Almasan, A., Almonte-Becerril, M., Amano, A., Amaravadi, R., Amarnath, S., Amer, A.O., Andrieu-Abadie, N., Anantharam, V., Ann, D.K., Anoopkumar-Dukie, S., Aoki, H., Apostolova, N., Auberger, P., Baba, M., Backues, S.K., Baehrecke, E.H., Bahr, B.A., Bai, X.Y., Bailly, Y., Baiocchi, R., Baldini, G., Balduini, W., Ballabio, A., Bamber, B.A., Bampton, E.T., Banhegyi, G., Bartholomew, C.R., Bassham, D.C., Bast Jr., R.C., Batoko, H., Bay, B.H., Beau, I., Bechet, D.M., Begley, T.J., Behl, C., Behrends, C., Bekri, S., Bellaire, B., Bendall, L.J., Benetti, L., Berliocchi, L., Bernardi, H., Bernassola, F., Besteiro, S., Bhatia-Kissova, I., Bi, X., Biard-Piechaczyk, M., Blum, J.S., Boise, L.H., Bonaldo, P., Boone, D.L., Bornhauser, B.C., Bortoluci, K.R., Bossis, I., Bost, F., Bourquin, J.P., Boya, P., Boyer-Guittaut, M., Bozhkov, P.V., Brady, N.R., Brancolini, C., Brech, A., Brenman, J.E., Brennand, A., Bresnick, E.H., Brest, P., Bridges, D., Bristol, M.L., Brookes, P.S., Brown, E.J., Brumell, J.H., Brunetti-Pierri, N., Brunk, U.T., Bulman, D.E., Bultman, S.J., Bultynck, G., Burbulla, L.F., Bursch, W., Butchar, J.P., Buzgariu, W., Bydlowski, S.P.,

Cadwell, K., Cahova, M., Cai, D., Cai, J., Cai, Q., Calabretta, B., Calvo-Garrido, J., Camougrand, N., Campanella, M., Campos-Salinas, J., Candi, E., Cao, L., Caplan, A.B., Carding, S.R., Cardoso, S.M., Carew, J.S., Carlin, C.R., Carmignac, V., Carneiro, L.A., Carra, S., Caruso, R.A., Casari, G., Casas, C., Castino, R., Cebollero, E., Cecconi, F., Celli, J., Chaachouay, H., Chae, H.J., Chai, C.Y., Chan, D.C., Chan, E.Y., Chang, R.C., Che, C.M., Chen, C.C., Chen, G.C., Chen, G.Q., Chen, M., Chen, Q., Chen, S.S., Chen, W., Chen, X., Chen, X., Chen, X., Chen, Y.G., Chen, Y., Chen, Y., Chen, Y.J., Chen, Z., Cheng, A., Cheng, C.H., Cheng, Y., Cheong, H., Cheong, J.H., Cherry, S., Chess-Williams, R., Cheung, Z.H., Chevet, E., Chiang, H.L., Chiarelli, R., Chiba, T., Chin, L.S., Chiou, S.H., Chisari, F.V., Cho, C.H., Cho, D.H., Choi, A.M., Choi, D., Choi, K.S., Choi, M.E., Chouaib, S., Choubey, D., Choubey, V., Chu, C.T., Chuang, T.H., Chueh, S.H., Chun, T., Chwae, Y.J., Chye, M.L., Ciarcia, R., Ciriolo, M.R., Clague, M.J., Clark, R.S., Clarke, P.G., Clarke, R., Codogno, P., Coller, H.A., Colombo, M.I., Comincini, S., Condello, M., Condorelli, F., Cookson, M.R., Coombs, G.H., Coppens, I., Corbalan, R., Cossart, P., Costelli, P., Costes, S., Coto-Montes, A., Couve, E., Coxon, F.P., Cregg, J.M., Crespo, J.L., Cronje, M.J., Cuervo, A.M., Cullen, J.J., Czaja, M.J., D'Amelio, M., Darfeuille-Michaud, A., Davids, L.M., Davies, F.E., De, F.M., de Groot, J.F., de Haan, C.A., De, M.L., De, M.A., De, T.V., Debnath, J., Degterev, A., Dehay, B., Delbridge, L.M., Demarchi, F., Deng, Y.Z., Dengjel, J., Dent, P., Denton, D., Deretic, V., Desai, S.D., Devenish, R.J., Di, G.M., Di, P.G., Di, P.C., Diaz-Araya, G., Diaz-Laviada, I., Diaz-Meco, M.T., Diaz-Nido, J., Dikic, I., Dinesh-Kumar, S.P., Ding, W.X., Distelhorst, C.W., Diwan, A., Djavaheri-Mergny, M., Dokudovskaya, S., Dong, Z., Dorsey, F.C., Dosenko, V., Dowling, J.J., Doxsey, S., Dreux, M., Drew, M.E., Duan, Q., Duchosal, M.A., 2012. Guidelines for the use and interpretation of assays for monitoring autophagy. Autophagy 8, 445–544.

Lau, K.F., Miller, C.C., Anderton, B.H., Shaw, P.C., 1999. Expression analysis of glycogen synthase kinase-3 in human tissues. J. Pept. Res. 54, 85–91.

Lee, J.H., Yu, W.H., Kumar, A., Lee, S., Mohan, P.S., Peterhoff, C.M., Wolfe, D.M., Martinez-Vicente, M., Massey, A.C., Sovak, G., Uchiyama, Y., Westaway, D., Cuervo, A.M., Nixon, R.A., 2010. Lysosomal proteolysis and autophagy require presenilin 1 and are disrupted by Alzheimer-related PS1 mutations. Cell 141, 1146–1158.

Lee, S., Sato, Y., Nixon, R.A., 2011. Lysosomal proteolysis inhibition selectively disrupts axonal transport of degradative organelles and causes an Alzheimer's-like axonal dystrophy. J. Neurosci. 31, 7817–7830.

Leroy, K., Ando, K., Heraud, C., Yilmaz, Z., Authelet, M., Boeynaems, J.M., Buee, L., De, D.R., Brion, J.P., 2010. Lithium treatment arrests the development of neurofibrillary tangles in mutant tau transgenic mice with advanced neurofibrillary pathology. J. Alzheimers Dis. 19, 705–719.

Leroy, K., Boutajangout, A., Authelet, M., Woodgett, J.R., Anderton, B.H., Brion, J.P., 2002. The active form of glycogen synthase kinase-3beta is associated with granulovacuolar degeneration in neurons in Alzheimer's disease. Acta Neuropathol. 103, 91–99.

Lesort, M., Jope, R.S., Johnson, G.V., 1999. Insulin transiently increases tau phosphorylation: involvement of glycogen synthase kinase-3beta and Fyn tyrosine kinase. J. Neurochem. 72, 576–584.

Li, X., Lu, F., Tian, Q., Yang, Y., Wang, Q., Wang, J.Z., 2006. Activation of glycogen synthase kinase-3 induces Alzheimer-like tau hyperphosphorylation in rat hippocampus slices in culture. J. Neural Transm. 113, 93–102.

Lovestone, S., Hartley, C.L., Pearce, J., Anderton, B.H., 1996. Phosphorylation of tau by glycogen synthase kinase-3 beta in intact mammalian cells: the effects on the organization and stability of microtubules. Neuroscience 73, 1145–1157.

Lovestone, S., Reynolds, C.H., Latimer, D., Davis, D.R., Anderton, B.H., Gallo, J.M., Hanger, D., Mulot, S., Marquardt, B., Stabel, S., 1994. Alzheimer's disease-like phosphorylation of the microtubule-associated protein tau by glycogen synthase kinase-3 in transfected mammalian cells. Curr. Biol. 4, 1077–1086.

Lucas, J.J., Hernandez, F., Gomez-Ramos, P., Moran, M.A., Hen, R., Avila, J., 2001. Decreased nuclear beta-catenin, tau hyperphosphorylation and neurodegeneration in GSK-3beta conditional transgenic mice. EMBO J. 20, 27–39.

Medina, M., Wandosell, F., 2011. Deconstructing GSK-3: the fine regulation of its activity. Int. J. Alzheimers Dis. 2011, 479249.

Mortimore, G.E., Poso, A.R., Lardeux, B.R., 1989. Mechanism and regulation of protein degradation in liver. Diabetes Metab. Rev. 5, 49–70.

Nijholt, D.A., de Graaf, T.R., van Haastert, E.S., Oliveira, A.O., Berkers, C.R., Zwart, R., Ovaa, H., Baas, F., Hoozemans, J.J., Scheper, W., 2011a. Endoplasmic reticulum stress activates autophagy but not the proteasome in neuronal cells: implications for Alzheimer's disease. Cell Death Differ. 18, 1071–1081.

Nijholt, D.A., De, K.L., Elfrink, H.L., Hoozemans, J.J., Scheper, W., 2011b. Removing protein aggregates: the role of proteolysis in neurodegeneration. Curr. Med. Chem. 18, 2459–2476.

Nijholt, D.A.T., van Haastert, E.S., Rozemuller, A.J.M., Scheper, W., Hoozemans, J.J.M., 2011c. The unfolded protein response is associated with early tau pathology in the hippocampus of tauopathies. J. Pathol. 226, 693–702.

Nixon, R.A., Wegiel, J., Kumar, A., Yu, W.H., Peterhoff, C., Cataldo, A., Cuervo, A.M., 2005. Extensive involvement of autophagy in Alzheimer disease: an immuno-electron microscopy study. J. Neuropathol. Exp. Neurol. 64, 113–122.

Noble, W., Planel, E., Zehr, C., Olm, V., Meyerson, J., Suleman, F., Gaynor, K., Wang, L., LaFrancois, J., Feinstein, B., Burns, M., Krishnamurthy, P., Wen, Y., Bhat, R., Lewis, J., Dickson, D., Duff, K., 2005. Inhibition of glycogen synthase kinase-3 by lithium correlates with reduced tauopathy and degeneration in vivo. Proc. Natl. Acad. Sci. U. S. A 102, 6990–6995.

Rankin, C.A., Sun, Q., Gamblin, T.C., 2008. Pre-assembled tau filaments phosphorylated by GSK-3b form large tangle-like structures. Neurobiol. Dis. 31, 368–377.

Ryves, W.J., Fryer, L., Dale, T., Harwood, A.J., 1998. An assay for glycogen synthase kinase 3 (GSK-3) for use in crude cell extracts. Anal. Biochem. 264, 124–127.

Schroder, M., Kaufman, R.J., 2005. ER stress and the unfolded protein response. Mutat. Res. 569, 29–63.

Sereno, L., Coma, M., Rodriguez, M., Sanchez-Ferrer, P., Sanchez, M.B., Gich, I., Agullo, J.M., Perez, M., Avila, J., Guardia-Laguarta, C., Clarimon, J., Lleo, A., Gomez-Isla, T., 2009. A novel GSK-3beta inhibitor reduces Alzheimer's pathology and rescues neuronal loss in vivo. Neurobiol. Dis. 35, 359–367.

Song, L., De, S.P., Jope, R.S., 2002. Central role of glycogen synthase kinase-3beta in endoplasmic reticulum stress-induced caspase-3 activation. J. Biol. Chem. 277, 44701–44708.

Susan, P.P., Dunn Jr., W.A., 2001. Starvation-induced lysosomal degradation of aldolase B requires glutamine 111 in a signal sequence for chaperone-mediated transport. J. Cell Physiol. 187, 48–58.

Takashima, A., Honda, T., Yasutake, K., Michel, G., Murayama, O., Murayama, M., Ishiguro, K., Yamaguchi, H., 1998. Activation of tau protein kinase I/glycogen synthase kinase-3beta by amyloid beta peptide (25-35) enhances phosphorylation of tau in hippocampal neurons. Neurosci. Res. 31, 317–323.

Tang, Q., Cai, J., Shen, D., Bian, Z., Yan, L., Wang, Y.X., Lan, J., Zhuang, G.Q., Ma, W.Z., Wang, W., 2009. Lysosomal cysteine peptidase cathepsin L protects against cardiac hypertrophy through blocking AKT/GSK3beta signaling. J. Mol. Med. (Berl) 87, 249–260.

Unterberger, U., Hoftberger, R., Gelpi, E., Flicker, H., Budka, H., Voigtlander, T., 2006. Endoplasmic reticulum stress features are prominent in Alzheimer disease but not in prion diseases in vivo. J. Neuropathol. Exp. Neurol. 65, 348–357.

Wagner, U., Utton, M., Gallo, J.M., Miller, C.C., 1996. Cellular phosphorylation of tau by GSK-3 beta influences tau binding to microtubules and microtubule organisation. J. Cell Sci. 109, 1537–1543.

Woodgett, J.R., 1990. Molecular cloning and expression of glycogen synthase kinase-3/factor A. EMBO J. 9, 2431–2438.

Yao, H.B., Shaw, P.C., Wong, C.C., Wan, D.C., 2002. Expression of glycogen synthase kinase-3 isoforms in mouse tissues and their transcription in the brain. J. Chem. Neuroanat. 23, 291–297.

Yorimitsu, T., Nair, U., Yang, Z., Klionsky, D.J., 2006. Endoplasmic reticulum stress triggers autophagy. J. Biol. Chem. 281, 30299–30304.